Journal of Materials Chemistry B

ROYAL SOCIETY OF CHEMISTRY

PAPER

View Article Online
View Journal

Cite this: DOI: 10.1039/c9tb02773d

A silver nanoparticle-assisted signal amplification electrochemiluminescence biosensor for highly sensitive detection of mucin 1†

Yu-Ping Wei,‡ Yi-Wen Zhang‡ and Chang-Jie Mao *

Received 7th December 2019,
Accepted 12th February 2020

DOI: 10.1039/c9tb02773d

rsc.li/materials-b

A novel electrochemiluminescence (ECL) biosensor was developed in this study, which was based on the Ag-NP modified tetrahedral DNA nanostructure. First, a stable and rigid three-dimensional tetrahedral DNA nanostructure (TDN) was modified on a gold electrode, which was used as a capture element. The TDN improves the accuracy and sensitivity of this biosensor. In addition, silver nanoparticles (Ag NPs) with excellent electrical conductivity were introduced on the edges of TDNs to enhance the ECL intensity of the metal–organic framework (MOF) nanomaterial. Apart from imparting conductivity, the Ag NPs can also act as co-reactant accelerators to enhance the ECL intensity. A Eu^{3+} doped Zr-MOF material (Eu@MOF) was proposed and used as an ECL material for the first time. Terminal phosphate-modified MUC1 aptamer DNA bonded with the exposed Zr nodes on the surface of MOFs through Zr–O–P bonds to construct the DNA–Eu@MOF signal element. Based on the Ag NP-modified TDN capture element and the DNA–Eu@MOF signal element, a hypersensitive biosensor was established. Under the optimal conditions, this biosensor exhibited a wide detection range from 1.135 fg mL^{-1} to 0.1135 ng mL^{-1} and a low detection limit of 0.37 fg mL^{-1} (S/N = 3) toward the target MUC1. The biosensor also showed excellent stability and high selectivity for MUC1 detection.

Introduction

Mucin 1 (MUC1) is a large glycoprotein which is produced in epithelial tissues, such as the mammary glands and respiratory, gastrointestinal, urinary and reproductive tracts.[1–3] MUC1 is expressed in normal cells and can be found in healthy human serum (<31 U mL^{-1}).[4] According to previous reports,[5–7] MUC1 is overexpressed in some cancers including colon, breast, ovarian and pancreatic cancer. Hence, MUC1 is a crucial biomarker for early cancer detection. Fluorescence enzyme-linked immunosorbent assay (ELISA), colorimetric methods, and electrochemical methods have been developed for MUC1 detection.[8–11] Compared with these methods, electrochemiluminescence (ECL) technology is a powerful tool for the detection of MUC1 due to the advantages of low background signal, easy controllability and simple equipment requirement.[12–15] However, improving detection sensitivity is still a research hotspot for trace sample detection, especially for the detection of the target in complex biological samples such as blood. The development of highly efficient ECL materials and signal amplification techniques can improve the sensitivity of the ECL sensor. In the past few years, various ECL materials have been identified, including $Ru(bpy)_3^{2+}$, luminol, noble-metal nanoclusters, quantum dots, carbon materials and metal–organic framework (MOF) materials.[16] MOF nanomaterials have gained importance in recent years and are known for their chemical stability, structural flexibility, easy modification and biocompatibility.[17–20] MOFs have been widely used in the sensor field, for example, Zhao *et al.* proposed a dual-quenching ECL strategy based on 3D MOFs for ultrasensitive detection of amyloid-β;[21] Dong *et al.* built an ECL immunosensor for sensitive detection of diethylstilbestrol based on UiO-67 MOFs,[22] and a stable ultrathin 2D MOF layer with excellent ECL properties was used to build a hypersensitive aptasensor for the MUC1 detection.[23] In order to further improve the ECL properties of MOF materials, we modified the MOF materials with lanthanides. Lanthanide functionalized-MOFs (Ln-MOFs) have received great interest in chemical sensing applications due to their excellent optical properties through multiple luminescent centers and well-defined porosity of MOFs.[24] These unique optical properties are attributed to the 4f electronic configuration of lanthanides, including a large Stokes shift, extremely sharp emission, long luminescence lifetimes and high quantum yields. The luminescent centers of Ln-MOFs not only include lanthanide nodes, but

Anhui Province Key Laboratory of Chemistry for Inorganic/Organic Hybrid Functionalized Materials, School of Chemistry & Chemical Engineering, Anhui University, Hefei 230601, P. R. China. E-mail: maochangjie@sina.com

† Electronic supplementary information (ESI) available: Materials and apparatus, feasibility of the biosensor, optimization of the detection conditions, and additional information as noted in the text. See DOI: 10.1039/c9tb02773d

‡ These authors contributed equally to this work.

also organic linkers and ligand–metal charge transfer.[25] However, Ln-MOFs have not been studied in the field of ECL. Here, we have studied the ECL performance of the Eu^{3+} doped Zr-MOF nanomaterial and built a biosensor based on it.

The signal amplification strategy is another important way of improving the sensitivity of ECL sensors, which has attracted considerable attention recently. The existing signal amplification technologies, such as the use of new redox-active probes, increasing the loading of labels, enzyme-assisted signal amplification process and DNA amplification techniques,[26] can meet the demand to a certain extent, but the complicated procedures, high cost and rigorous conditions limit the widespread application of these methods. With regard to DNA amplification technology, the introduction of DNA nanotechnology is a good way of eliminating the above limitations. For example, Wen and co-workers developed an electrochemical sensor based on tetrahedral DNA nanostructures (TDNs) and reduced the detection limit of cocaine to 33 nM.[27] TDNs are artificial self-assembled three-dimensional DNA nanostructures with the advantages of convenient synthesis, high yield, high structural stability and excellent mechanical rigidity.[28] Despite these advantages, one main limitation of TDNs is the poor conductivity in the electrochemical biosensor. In order to overcome the problem of weak conductivity of TDNs, we introduced silver nanoparticles (Ag NPs) *in situ* on the edges of TDNs. In addition to accelerating electron transfer, Ag NPs can also act as a co-reactant accelerator to further increase the ECL intensity.[29,30] In this study, it was verified that an ultrasensitive biosensor could be constructed by combining Eu@MOF materials and TDN signal amplification technology.

In this research, we developed a hypersensitive ECL biosensor for the detection of MUC1, which was based on the Ag-NP-modified TDN capturing component and an aptamer-mediated MOF signal element. First, the Ag NP-modified TDN was fixed on the gold electrode. The capture DNA modified on the top vertex of the TDN was specifically recognized by the DNA–Eu@MOF. The Eu@MOF then exhibited an ECL response for this biosensor. When the target, MUC1, was incubated with the biosensor, MUC1 combined with the aptamer and removed the DNA–Eu@MOF from the electrode. The ECL response signal of the biosensor becomes weaker as the DNA–Eu@MOF is removed. The schematic for the construction process of the ECL biosensor is shown in Scheme 1.

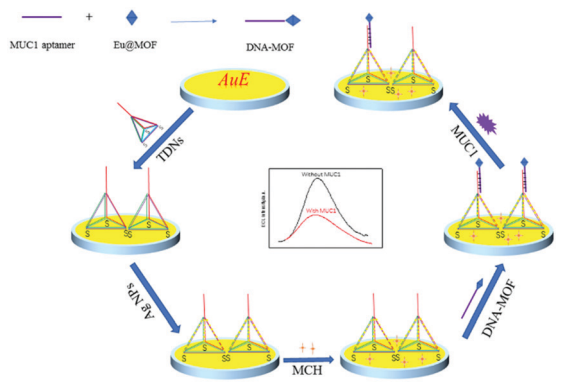

Scheme 1 A schematic diagram of the development of the ECL biosensor.

Experimental

Materials and apparatus are included in the ESI.†

Preparation of $H_2TCPP \subset UiO\text{-}66\text{-}2,5\text{-}(COOH)_2$ and $Eu@H_2TCPP \subset UiO\text{-}66\text{-}2,5\text{-}(COOH)_2$

$H_2TCPP \subset UiO\text{-}66\text{-}2,5\text{-}(COOH)_2$ (MOF) was prepared according to the method outlined in previous studies.[31] First, TCPP was synthesized as shown in a previous report.[32] A total of 5 mg of TCPP, 100 mg of $ZrCl_4$ and 120 mg H_4BTe_4 were dispersed in a Pyrex vial containing 2 mL DMF, 0.1 mL H_2O and 0.3 mL TFA. The contents of the Pyrex vial were ultrasonically dissolved and then the mixture was heated in an oven at 135 °C for 24 h. After cooling to room temperature, a pink solid was obtained by centrifugation. The obtained MOF was then washed three times with DMF and ethanol, and dried in an oven at 80 °C.

H_2TCPP-UiO-66 was synthesized by a hydrothermal method. A total of 30 mg $ZrCl_4$, 10 mg TCPP, 30 mg BDC and 500 mg BA were ultrasonically dissolved in 2 mL DMF in a Pyrex vial. The contents of the Pyrex vial were then heated in an oven at 135 °C for 24 h.

$Eu@H_2TCPP \subset UiO\text{-}66\text{-}2,5\text{-}(COOH)_2$ (Eu@MOF) was synthesized according to a previously described procedure.[33] Fifty milligrams of the MOF was dispersed in 20 mL $Eu(NO)_3$ solution, and the mixture was stirred at 60 °C for 24 h. The solid was then collected by centrifugation, washed with distilled water, and collected by drying under vacuum at 60 °C.

Preparation of aptamer-$Eu@H_2TCPP \subset UiO\text{-}66\text{-}2,5\text{-}(COOH)_2$

According to a previous report,[34] the collected Eu@MOF was re-dispersed in distilled water. MOF solution (0.3 mL) was mixed with 0.5 mL DNA solution, and the mixture was oscillated vigorously overnight. Then, 100 μL HEPES buffer (1 M, pH 7.4) and 50 μL NaCl (2 M) solution were added to the mixture under stirring. Following incubation, the DNA–Eu@MOF was purified by centrifugation. Finally, the DNA–Eu@MOF was dispersed in TE buffer and then stored at 4 °C until use.

Preparation of TDNs

TDNs were synthesized according to a previous study.[35] Briefly, S1, S2, S3, and S4 were mixed with TM buffer and 30 mM TCEP solution, and then the mixture was incubated at 37 °C for 1 h. The mixture was heated at 95 °C for 10 min and immediately cooled down to 4 °C to form stable TDNs.

Pretreatment of the gold electrode

The gold electrode was polished with alumina powder and cleaned with deionized water and ethanol in turns for further use. The gold electrode was then pretreated with 20 μL piranha solution (98% H_2SO_4 : 30% H_2O_2 = 7 : 3) to clean the electrode surface. The gold electrode was then tested by cyclic voltammetry (CV) in 0.5 M H_2SO_4 solution to obtain a reproducible curve.

Finally, the gold electrode was douched with distilled water and dried with N_2.

Fabrication of the ECL biosensor

First, 10 μL TDNs were added to the cleaned gold electrode and incubated at 4 °C overnight. After flushing with PBS buffer and drying with N_2, 10 μL $AgNO_3$ solution (0.1 M) was added to the gold electrode and incubated for 15 min to fix Ag^+ onto the DNA backbone. After 15 min, the gold electrode was washed with PBS buffer and dried with N_2. 10 μL hydroquinone solution (0.05 M) was added to the gold electrode to reduce the Ag^+ on the DNA backbone. The Ag NPs were grown in citrate solution (1 mM $AgNO_3$, 2 mM hydroquinone, 0.1 M sodium citrate, pH 3.5) for 8 min under dark conditions. After washing with PBS buffer and drying with N_2, the Ag NP-TDNs were successfully modified on the gold electrode. In order to prevent nonspecific adsorption, 10 μL MCH (1 mM) was added to the electrode, and incubated at 37 °C for 30 min. After rinsing and drying, the gold electrode was incubated with 10 μL DNA–Eu@MOF at 37 °C for 2 h. The electrode was then washed with PBS buffer and stored at 4 °C until use.

ECL measurement procedure

The modified electrode was incubated with different concentrations of MUC1 solutions at 30 °C for 50 min. The electrode was then rinsed with PBS buffer to remove the unbound MUC1. Finally, the electrode was analysed using an ECL analyzer in PBS buffer containing 0.12 M $K_2S_2O_8$. The voltage of the photomultiplier tube was 800 V.

Results and discussion

Characterization of the MOF and Eu@MOF

The morphology and size of the Eu@MOF were characterized by scanning electron microscopy (SEM). As shown in Fig. S1 (ESI†), the spherical Eu@MOF particles were approximately 100 nm in size and had a uniform morphology and size. Fig. S2 (ESI†) shows the EDS-element mapping results of the Eu@MOF. Clearly, Eu elements distribute uniformly in the MOF material.

The crystal structures of the MOF and Eu@MOF were verified by powder X-ray diffraction (PXRD) and the PXRD patterns are shown in Fig. 1A. Compared with the simulated UiO-66 (curve a),[31] the PXRD peak of experimental UiO-66 (curve b) showed no significant change, indicating that UiO-66 was successfully synthesized. When H_2TCPP (curve c) was incorporated into the UiO-66, there was almost no further change in the diffraction peaks. After the introduction of carboxyl group (curve d) and Eu^{3+} (curve e) into the H_2TCPP⊂UiO-66, the organic nano-metal frame still retained its crystallinity.

The as-prepared UiO-66 was also characterized by Fourier transform infrared spectrometry as shown in Fig. 1B. Compared with H_2TCPP⊂UiO-66 (curve a), for H_2TCPP⊂UiO-66-2,5-$(COOH)_2$ (curve b) a visible absorption peak of free –COOH was observed at 1658 cm^{-1}.[33] Following the combination with Eu^{3+} (curve c), the absorption peak strength of free –COOH reduced significantly, as some of the carboxyl functional groups combined with Eu^{3+}.

In order to further demonstrate that the Eu^{3+} was coordinated to the free carboxyl, X-ray photoelectron spectroscopy (XPS) analyses were performed. As shown in Fig. 2A, there was a characteristic peak of Eu 3d at 1135 eV in Eu@MOF (curve b). After incorporation of Eu^{3+}, the O1s characteristic peak of free carboxyl oxygen atoms (Fig. 2B) at 531.75 eV in curve a was shifted to 532 eV (curve b), indicating the existence of a coordination interaction between Eu^{3+} and free oxygen of the carboxyl group.[36]

Characterization of the DNA–Eu@MOF

The hydrodynamic size of the Eu@MOF measured by dynamic light scattering (DLS) (Fig. 2C) was 126.4 nm, which matched the SEM results. After combining with the oligonucleotides, the hydrodynamic size increased from 126.4 nm to 151.8 nm, and this increase was due to the shell thickness of the single stranded DNA. In order to prove that the DNA was successfully linked to the Eu@MOF, the zeta potential was measured and is shown in Fig. 2D. The zeta potential of the individual Eu@MOF was −11.6 mV, the zeta potential of the DNA–Eu@MOF was −30.8 mV and the difference between the potentials of Eu@MOF and DNA–Eu@MOF was due to the negatively charged DNA (zeta potential was −17.3 mV).

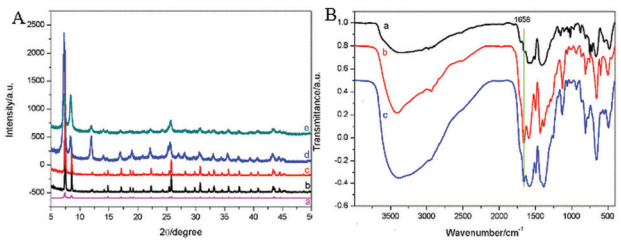

Fig. 1 (A) PXRD patterns of (a) UiO-66 simulated, (b) UiO-66, (c) H_2TCPP⊂UiO-66, (d) H_2TCPP⊂UiO-66-2,5-$(COOH)_2$, and (e) Eu@MOF; (B) FTIR spectra of (a) H_2TCPP⊂UiO-66, (b) H_2TCPP⊂UiO-66-2,5-$(COOH)_2$, and (c) Eu@MOF.

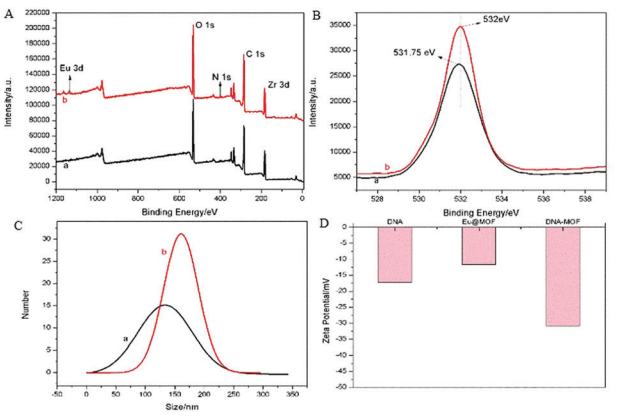

Fig. 2 (A) XPS spectra of the full region of (a) H_2TCPP⊂UiO-66-2,5-$(COOH)_2$ and (b) Eu@MOF; (B) O 1s characteristic peaks of (a) H_2TCPP⊂UiO-66-2,5-$(COOH)_2$ and (b) Eu@MOF; (C) dynamic light scattering spectra of (a) Eu@MOF and (b) DNA–Eu@MOF; and (D) zeta potential of (a) Eu@MOF, (b) DNA, and (c) DNA–Eu@MOF.

Characterization of TDNs and Ag NPs

AFM was performed to further confirm the successful formation of TDNs. The newly synthesized TDNs and Ag NP-modified TDNs were pipetted onto the cleaned gold electrode for observation by AFM. The AFM image is shown in Fig. 3A, uniformly sized triangles were observed on the gold surface. Following the Ag NP growth, the size of the triangles significantly increased (Fig. 3B). The cyclic voltammetry test (Fig. S2B, ESI†) could also prove that Ag NPs were successfully modified on the edges of TDNs.

Feasibility of the biosensor

EIS and CV were employed to verify the fabrication of the biosensor and the results are shown in the ESI.†

Optimization of the experimental conditions

In order to obtain the best detection of MUC1, a series of conditions for this biosensor were optimized, including the concentration of the co-reactant $K_2S_2O_8$, the incubation time and temperature of the DNA–Eu@MOF, and the incubation time and temperature of MUC1. The optimization of the experimental conditions is shown in the ESI.†

Performance of the biosensor for the detection of MUC1

The detection of MUC1 was carried out under the optimal conditions. As shown in Fig. 4A, the ECL intensity clearly decreased when the MUC1 concentration ranged from 1.135 fg mL^{-1} to 0.1135 ng mL^{-1}. It can be seen in Fig. 4B that the ECL response was proportional to the logarithm of the MUC1 concentration from 1.135 fg mL^{-1} to 0.1135 ng mL^{-1}. The regression equation of the biosensor is as follows: $I = -789.84 \lg C + 3497.32$

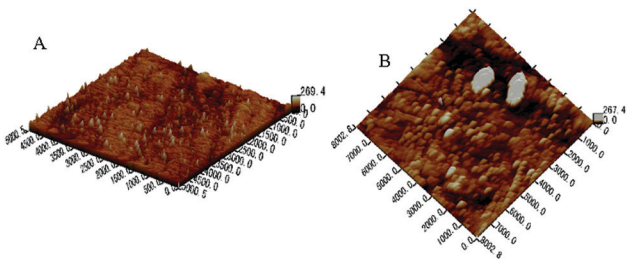

Fig. 3 (A) Atomic force microscopy images of TDNs and (B) Ag NP modified TDNs.

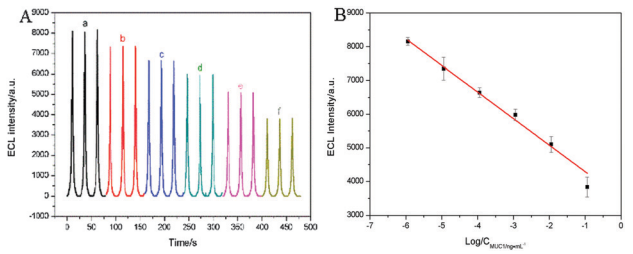

Fig. 4 (A) ECL response and (B) calibration curves for different MUC1 levels ((a) 1.135 fg mL^{-1}, (b) 11.35 fg mL^{-1}, (c) 0.1135 pg mL^{-1}, (d) 1.135 pg mL^{-1}, (e) 11.35 pg mL^{-1}, and (f) 0.1135 ng mL^{-1}).

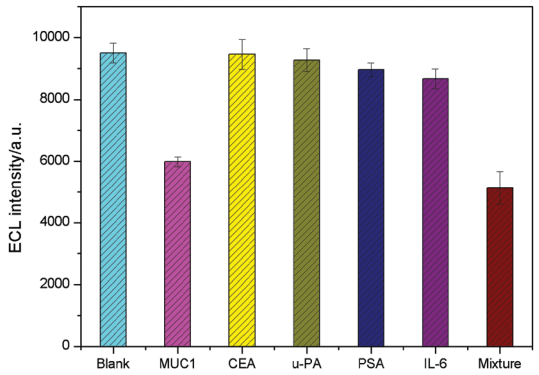

Fig. 5 Selectivity of the ECL biosensor for different targets from left to right: blank sample, 1.135 pg mL^{-1} MUC1, 100 pg mL^{-1} CEA, 100 pg mL^{-1} uPA, 100 pg mL^{-1} PSA, 100 pg mL^{-1} IL-6 and the mixture sample (containing 1.135 pg mL^{-1} MUC1, 100 pg mL^{-1} CEA, 100 pg mL^{-1} uPA, 100 pg mL^{-1} PSA, and 100 pg mL^{-1} IL-6).

(correlation coefficient of 0.994), and the detection limit was 0.37 fg mL^{-1} (S/N = 3). Compared with previous studies (Table S1 ESI†), our biosensor showed a lower detection limit. These results indicated that this biosensor exhibits excellent sensitivity to the target.

Selectivity and stability of the biosensor

Selectivity is an important factor for an excellent biosensor. As shown in Fig. 5, the selectivity of the proposed biosensor was examined under the optimal conditions by including the following additional proteins at 0.1 ng mL^{-1}: CEA, u-PA, PSA, and IL-6. The ECL intensities of these proteins were not significantly different compared with that of the blank sample. For the mixed samples (containing 0.1 ng mL^{-1} u-PA, PSA, CEA, IL-6 and 1.135 pg mL^{-1} MUC1), the biosensor response was similar to that for 1.135 pg mL^{-1} MUC1. These results indicated that the proposed biosensor showed selectivity and specificity for the detection of MUC1. The stability of the developed biosensor was tested by storing the electrode at 4 °C for two weeks, and the ECL response was found to change only slightly (98.2% of its initial intensity).

Application in the detection of real samples

For the purpose of evaluating the analytical reliability and application potential of the proposed biosensor, the MUC1 standard added to healthy human serum was detected. First, human serum was diluted 10 times with PBS buffer. Then different concentrations of MUC1 were dispersed in human serum and detected using the biosensor. As shown in Table S2 (ESI†), the recovery levels were 99.56%, 100.41% and 94.45%, respectively. Therefore, the ECL biosensor has great potential for sensitive and accurate detection of MUC1 in real samples.

Conclusions

In this study, we developed a hypersensitive and specific ECL biosensor for the accurate detection of MUC1. First, a novel Eu^{3+} doped Zr-MOF was successfully synthesized. The Eu@MOF was

not only an excellent ECL emitter but also showed good biocompatibility. The terminal phosphate functionalized aptamer could immobilize on the Eu@MOF nanoparticle surface through Zr–O–P bonds. A three-dimensional DNA nanostructure was introduced into the ECL biosensor to improve its sensitivity. In order to avoid hindered electron transfer, Ag NPs were introduced into the TDN framework. Ag NPs can also improve the ECL intensity as a co-reactant accelerator. Based on the above conditions, a hypersensitive and specific ECL biosensor for MUC1 was developed. This biosensor exhibited a wide detection range from 1.135 fg mL^{-1} to 0.1135 ng mL^{-1}, and a low detection limit of 0.37 fg mL^{-1} for the target MUC1. The ECL biosensor not only exhibited outstanding performance in the detection of MUC1, but may also be feasible for the detection of other biomolecules by changing the specific recognition element.

Conflicts of interest

There are no conflicts to declare.

Acknowledgements

This work was supported by the National Natural Science Foundation of China (Grant No. 21976001) and the Open fund for Discipline Construction, Institute of Physical Science and Information Technology.

Notes and references

1 M. Frédéric, G. Luquet, B. Marie and D. Medakovic, *Curr. Top. Dev. Biol.*, 2008, **80**, 209–276.
2 C. L. Hattrup, S. J. Gendler and C. Hatrupp, *Annu. Rev. Physiol.*, 2008, **70**, 431–457.
3 S. J. Gendler and A. P. Spicer, *Annu. Rev. Physiol.*, 1995, **57**, 607–634.
4 M. S. Nabavinia, A. Gholoobi, F. Charbgoo, M. Nabavinia, M. Ramezani and K. Abnous, *Med. Res. Rev.*, 2017, **37**, 1518–1539.
5 Y. Niv, *World J. Gastroenterol.*, 2008, **14**, 2139–2141.
6 D. W. Kufe, *Nat. Rev. Cancer*, 2009, **9**, 874–885.
7 H. H. Jo, J. Her and C. Ban, *Biosens. Bioelectron.*, 2015, **71**, 129–136.
8 R. Falahat, M. Wiranowska, N. D. Gallant, D. Toomey, R. Hill and N. Alcantar, *Cell. Immunol.*, 2015, **298**, 96–103.
9 S. W. Liu, N. H. Xu, C. Y. Tan, W. Fang, Y. Tan and Y. Y. Jiang, *Anal. Chim. Acta*, 2018, **1018**, 86–93.
10 W. T. Yang, Y. Shen, D. Zhang and W. J. Xu, *Chem. Commun.*, 2018, **54**, 10195–10198.
11 C. Y. Lin, H. X. Zheng, Y. Y. Huang, R. Yuan and Y. Q. Chai, *Biosens. Bioelectron.*, 2018, **117**, 474–479.
12 J. Wang, Y. Zhuo, Y. Zhou, H. J. Wang, R. Yuan and Y. Q. Chai, *ACS Appl. Mater. Interfaces*, 2016, **8**, 12968–12975.
13 H. Ke, H. Sha, Y. Wang, W. Guo, X. Zhang, Z. Wang, C. Huang and N. Jia, *Biosens. Bioelectron.*, 2017, **100**, 266–273.
14 W. Wen, X. Yan, C. Zhu, D. Du and Y. Lin, *Anal. Chem.*, 2017, **89**, 138–156.
15 G. B. Hu, C. Y. Xiong, W. B. Liang, X. S. Zeng, H. L. Xu, Y. Yang, L. Y. Yao, R. Yuan and D. R. Xiao, *ACS Appl. Mater. Interfaces*, 2018, **10**, 15913–15919.
16 L. L. Hou and B. B. Zhou, *Int. J. Electrochem. Sci.*, 2019, **14**, 2489–2508.
17 L. J. Murray, M. Dinca and J. R. Long, *Chem. Soc. Rev.*, 2009, **38**, 1294–1314.
18 X. Lin, J. H. Jia, X. B. Zhao, K. M. Thomas, A. J. Blake, G. S. Walker and N. R. Champness, *Angew. Chem., Int. Ed.*, 2010, **118**, 7518–7524.
19 J. R. Li, R. J. Kuppler and H. C. Zhou, *Chem. Soc. Rev.*, 2009, **38**, 1477–1504.
20 S. Abednatanzi, P. G. Derakhshandeh, H. Depauw, F. X. Coudert, H. Vrielinck, P. V. D. Voort and K. Leus, *Chem. Soc. Rev.*, 2019, **48**, 2497–2658.
21 G. H. Zhao, Y. G. Wang, X. J. Li, Q. Yue, X. Dong, B. Du, W. Cao and Q. Wei, *Anal. Chem.*, 2019, **91**, 1989–1996.
22 X. Dong, G. Zhao, L. Liu, X. Li, Q. Wei and W. Cao, *Biosens. Bioelectron.*, 2018, **110**, 201–206.
23 Y. Yang, G. B. Hu, W. B. Liang, L. Y. Yao, W. Huang, R. Yuan and D. R. Xiao, *Nanoscale*, 2019, **11**, 10056–10063.
24 J. N. Hao and B. Yan, *Adv. Funct. Mater.*, 2017, **27**, 1603856.
25 Y. Zhou, H. H. Chen and B. Yan, *J. Mater. Chem. A*, 2014, **2**, 13691–13697.
26 C. F. Ding, W. Zhang, W. Wang, Y. Y. Chen and X. Q. Li, *Anal. Chem.*, 2015, **65**, 137–150.
27 Y. Wen, H. Pei, Y. Wan, Y. Su, Q. Huang, S. Song and C. H. Fan, *Anal. Chem.*, 2011, **83**, 7418–7423.
28 Y. Lin, J. P. Jia, R. Yang, D. Z. Chen, J. Wang, F. Luo, L. H. Guo, B. Qin and Z. Y. Lin, *Anal. Chem.*, 2019, **91**, 3717–3724.
29 T. Q. Yi, W. Gong, Y. M. Lei, W. J. Zeng, Y. Q. Chai, R. Yuan and Y. Zhuo, *J. Electrochem. Soc.*, 2018, **165**, B686–B693.
30 M. Jiao, G. F. Jie, L. Tan and S. Y. Niu, *Anal. Chim. Acta*, 2017, **983**, 166–172.
31 Y. Sun, L. X. Sun, D. W. Feng and H. C. Zhou, *Angew. Chem., Int. Ed.*, 2016, **128**, 6471–6475.
32 D. Feng, W. C. Chung, Z. Wei, Z. Y. Gu, H. L. Jiang, Y. P. Chen, D. J. Darensbourg and H. C. Zhou, *J. Am. Chem. Soc.*, 2013, **135**, 17105–17110.
33 J. N. Hao and B. Yan, *Chem. Commun.*, 2015, **51**, 7737–7740.
34 Z. Wang, Y. Fu, Z. Z. Kang, X. G. Liu, N. Chen, Q. Wang, Y. Q. Tu, L. H. Wang, S. P. Song, D. S. Ling, H. Y. Song, X. Q. Kong and C. H. Fan, *J. Am. Chem. Soc.*, 2017, **139**, 15784–15791.
35 Y. Lin, J. P. Jia, R. Yang, D. Z. Chen, J. Wang, F. Luo, L. H. Guo, B. Qin and Z. Y. Lin, *Anal. Chem.*, 2019, **91**, 3717–3724.
36 J. N. Hao and B. Yan, *Adv. Science News*, 2017, **27**, 1603856.